Determination of the transverse *X*-point effective mass in AlAs and its pressure dependence

Hyunsik Im,[1] P. C. Klipstein,[1,*] R. Grey,[2] and G. Hill[2]
[1]*Clarendon Laboratory, Department of Physics, University of Oxford, Parks Road, Oxford, OX1 3PU, United Kingdom*
[2]*Department of Electrical and Electronic Engineering, University of Sheffield, Mappin Street, Sheffield SI 3JD, United Kingdom*
(Received 20 March 2000)

We have investigated $2D \rightarrow 2D$ magnetotunneling in a GaAs/AlAs ''double barrier structure'' with 20 Å AlAs layers separated by a 40 Å GaAs layer, as a function of hydrostatic pressure and in the presence of a magnetic field perpendicular to the interfaces ($\mathbf{B} \| \mathbf{J}$). At $B=0$ and at high pressures ($\geqslant 10$ kbar), resonant tunneling and its phonon satellites are observed between a Γ symmetry state in the GaAs emitter and a longitudinal X_Z symmetry state in the AlAs collector. As the pressure is increased, the band offset between the Γ and the X_Z states is decreased, resulting in a shift of these resonances to lower bias. At $B \neq 0$, clear periodic structures are observed in the current vs voltage characteristic, which are interpreted as resonant tunneling from the lowest emitter Γ Landau level to X_Z collector levels of increasing Landau index. Quantitative analysis yields the energies of the phonons participating in the inelastic tunneling, and the transverse mass, m_{XY}, at the band edge of AlAs. Our method provides the most accurate determination to date of the transverse mass, and reports on its pressure dependence. We find $m_{XY}/m_0 = [(0.284 \pm 0.008) - (0.0039 \pm 0.0003) \times P]$ where P is the pressure in kbar.

I. INTRODUCTION

There has been a considerable amount of work over more than a decade, studying the properties of GaAs/Al_xGa_{1-x}As resonant tunneling structures in a magnetic field applied along the [001] growth direction (*z* direction). Almost all of this work has concerned tunneling between Landau levels (LL's) with Γ symmetry.[1,2] Such Γ states are associated with the center of the Brillouin zone. Within the past 5 years, however, the development of high pressure techniques has enabled considerable progress to be made in the understanding of states with *X* symmetry.[3–5] The X_X, X_Y, and X_Z minima are located, respectively, near the [100], [010], and [001] boundaries of the Brillouin zone. The $X_{X,Y}$ states exhibit clear $2D \rightarrow 2D$ tunneling, and a recent study of samples with 70 Å AlAs wells and a 40 Å GaAs barrier has shown a clear signature of Landau levels with $X_{X,Y}$ symmetry.[6]

It is very difficult to observe analogous resonant behavior between X_Z states, since the effective mass of the X_Z states is heavier and the tunneling is suppressed. Therefore it is necessary to use a very thin GaAs layer of around 20 Å. It is also necessary to employ samples consisting of AlAs layers thinner than ~50 Å, because the lowest confined states in AlAs layers thicker than ~50 Å are the $X_{X,Y}$ states, due to the competing effects of spatial confinement and compressive strain.[7] Recently we have reported results for a sample with 40 Å AlAs layers and a 20 Å GaAs layer, where we were able to observe LL's with X_Z symmetry at high pressure.[8] From these measurements an approximate value for the transverse effective mass was obtained: $m_{XY} = (0.25 \pm 0.03) m_0$. Values of $0.25m_0$ and $0.28m_0$, respectively, have also been obtained recently *with a similar precision*, from zero magnetic field measurements on structures exhibiting $X_{X,Y}$ tunneling[4] and from magnetotunneling in a single barrier structure.[9]

In this study, we report a third type of pressure-induced resonant magnetotunneling process in a GaAs/AlAs double barrier structure. It occurs between Γ states in the emitter accumulation layer and X_Z states in the collector AlAs layer. Thin AlAs layers, each of 20 Å, are used to allow sufficient overlap of the Γ emitter states with the X_Z collector states. The central GaAs layer is 40 Å. In low magnetic fields, we are able to observe clear peaks due to phonon assisted tunneling and to identify unambiguously in each case which phonons are involved. At high fields, we observe a fan of peaks associated with tunneling between the lowest Γ-symmetry LL in the emitter accumulation layer and up to six X_Z-symmetry LL's in the AlAs collector. By comparing the two sets of peaks and from a very precise knowledge of the zone center GaAs LO phonon, we are able to calibrate the cyclotron energy quite accurately. From this energy we make a new determination of the transverse effective mass m_{XY} at the *X* point of AlAs, which is more precise than previous determinations. We have also determined its pressure dependence. By taking this pressure dependence into account, the fairly wide range of values for the transverse effective mass discussed earlier can be explained.

An accurate knowledge of the transverse mass at pressures up to ~10 kbar is very important for the following reason. A recent observation of X_X-X_Y mixing *in* AlAs *quantum wells* demonstrated that the presently accepted **k·p** parameters for the *X*-point ''camel's back'' dispersion in AlAs must be changed substantially, in order to explain the mixing results.[10] Subsequently, a direct mapping of the camel's back minimum has been made, using magnetotunneling at ~10 kbar in a parallel magnetic field, from which the **k·p** parameters have been determined more accurately.[11,13] These measurements must be calibrated using a value for the transverse mass. The accuracy of this new determination thus depends directly on the precision of the present work. The new parameters lead to a camel's back, which is closer to the *X* point in wave vector and deeper in energy than the presently accepted one.[12] The Fermi surface at each *X* point is also

considerably more spherical than has previously been thought.

II. EXPERIMENT

The structure studied here was a symmetric *n-i-n* GaAs/AlAs ''double barrier structure'' grown by molecular beam epitaxy on [001]-oriented substrates and was processed into 20-μm-diam mesa devices, which were mounted in nonmagnetic packages. The structure consisted of the following layers: 0.25 μm $n=2.5\times10^{18}\,\mathrm{cm}^{-3}$ GaAs buffer, 0.5 μm $n=3.2\times10^{17}\,\mathrm{cm}^{-3}$ GaAs, 100 Å undoped GaAs spacer, 20 Å undoped AlAs, 40 Å undoped GaAs, 20 Å undoped AlAs, 100 Å undoped GaAs spacer, 0.5 μm $n=3.5\times10^{17}\,\mathrm{cm}^{-3}$ GaAs, and 0.25 μm $n=2.7\times10^{18}\,\mathrm{cm}^{-3}$ GaAs top contact. The doping levels were checked by electrochemical profiling. The layer thicknesses are expected to be correct to within a few angstroms, on the basis of a detailed calibration of similar samples from the same source.[4]

The measurements presented here were taken at a temperature of 4.2 K. The two terminal current-voltage measurements (I-V) were carried out using a combined voltage source and virtual ground current amplifier system. The conductance (dI/dV) and its first derivative (d^2I/dV^2) were measured by adding a 1 kHz sinusoid of 1 mV amplitude to the applied bias, and detecting the ac signal with a lock-in amplifier. Where indicated, d^2I/dV^2 was also measured by numerical differentiation of the first derivative data. Both methods gave second derivative results that were virtually indistinguishable from each other. Forward bias corresponds to a positive substrate potential.

Hydrostatic pressure was applied using a clamp cell, equipped with an *in situ* manganin wire manometer. The accuracy of pressure measurement was within ±0.2 kbar.[14]

III. RESULTS AND ANALYSIS

The bias dependence of the conductance (dI/dV) and the second derivative of the current (d^2I/dV^2) at 4.2 K and zero magnetic field are plotted as a function of pressure in Fig. 1. Two kinds of resonance are observed near zero bias, seen more clearly in the second derivative measurements. One is marked as solid arrows, the other as dashed arrows, in reverse bias [Fig. 1(b)]. There are two valuable pieces of information shown by these resonances. The pressure dependence of the resonances gives clear evidence of the emitter and collector states involved. Up to 14.7 kbar, the solid arrow resonances continue to move down in bias with increasing pressure. This means that increasing hydrostatic pressure makes the energy difference between the emitter and collector states become smaller. The other resonance first shows up at 13.7 kbar and its amplitude becomes large with increasing pressure. Its bias position remains nearly constant at ~-12 mV. This shows that the energy difference between the emitter and collector states for the dashed arrow resonance remains fixed with increasing pressure.

Figure 2 shows the Γ- and X-conduction band profiles under a small bias and at pressures before the type II transition. The Γ-conduction band profile shifts up at a rate of $\sim$13 meV/kbar (Ref. 4) with respect to the X profile. At zero bias, it crosses the lowest confined state in the X profile at the type

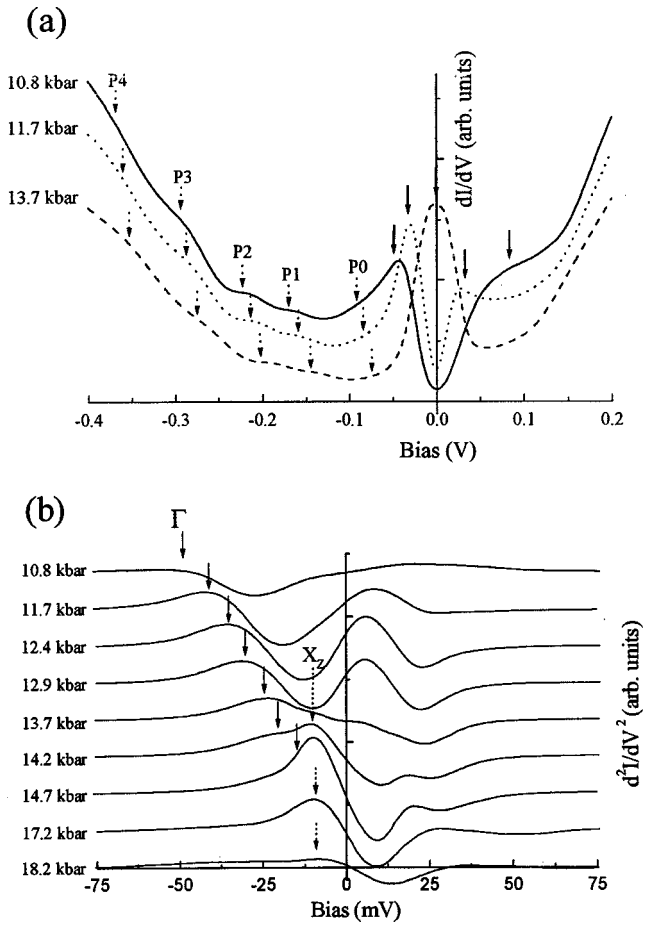

FIG. 1. (a) Conductance vs voltage (I'-V) at 4.2 K and at different pressures between 10.8 and 13.7 kbar. The black and gray solid arrows stand for $\Gamma\rightarrow X_Z(1)$ and phonon-assisted processes. (b) Pressure dependence of the second derivative of current vs voltage (I''-V). Note different bias scale. The solid and dashed arrows represent the $\Gamma\rightarrow X_Z(1)$ and $X_Z(1)\rightarrow X_Z(1)$ resonances, respectively.

II transition, which in our sample is around 14 kbar. Therefore, from the pressure-induced shifts in their bias positions, the solid and dashed arrow resonances in Fig. 1 can be attributed to $\Gamma\rightarrow X_Z(1)$ and $X_Z(1)\rightarrow X_Z(1)$ processes, respectively, where the final $X_Z(1)$ state resides in the collector AlAs layer. We believe that the mechanism of the $X_Z(1)\rightarrow X_Z(1)$ process is based on quantum beats, whose beat frequency is enhanced several orders of magnitude by Γ-X_Z mixing, as discussed elsewhere.[5,15] Thus it can be observed even though the central GaAs layer is quite thick.

Beyond these main resonances, peaks due to five phonon-assisted resonant tunneling processes, $P0-P4$, are well resolved in reverse bias, as may be seen in Fig. 1(a). As pressure is increased, these features shift downwards at a rate of $\sim-(13\pm2)$ mV/kbar, similar behavior to the $\Gamma\rightarrow X_Z(1)$ resonance. This fact confirms that these features are the phonon satellites of the $\Gamma\rightarrow X_Z(1)$ resonance. The only exception is $P4$ whose final state is $X_{XY}(1)$. This will be discussed further below. The band profiles for both the direct $\Gamma\rightarrow X_Z(1)$ process and its phonon satellites are shown schematically in Figs. 2(a) and 2(b), respectively. The wavy arrows in Fig. 2(b) represent two examples of a phonon-assisted resonance. Note that it is more probable that phonon

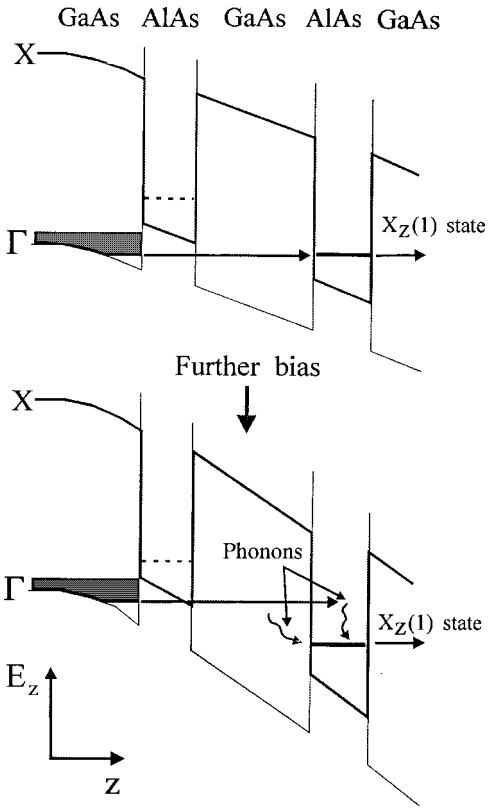

FIG. 2. Schematic representation of the Γ and X_Z conduction band profiles at $B=0$ just before the type II transition and biased to the $\Gamma \rightarrow X_Z(1)$ resonance (a) and to the $\Gamma \rightarrow X_Z(1)+$*phonon* resonance (b). The wavy arrows represent phonon emission.

emission for the inelastic tunneling process will occur in the central GaAs or collector AlAs layers as opposed to the emitter AlAs layer, since in the latter case the tunneling barrier height is larger by an amount equal to the phonon energy, resulting in a smaller electron tunneling probability.

At this point, it is necessary to explain more about the single conductance peak at zero bias. As pressure is increased beyond the type II transition where the $X_Z(1)$ state in the emitter AlAs layer is below the GaAs Γ-conduction band edge, an energy barrier δ is formed at the GaAs/AlAs emitter interface, and a small depletion layer of width W extends into the GaAs emitter. Both δ and W increase with pressure, as does the amount of charge in the X_Z quantum wells at zero bias. Thus one would expect that $\Gamma \rightarrow X_Z(1)$ becomes weaker, whereas $X_Z(1) \rightarrow X_Z(1)$ becomes more visible, with pressure. These features are clearly observed in the second derivative measurements in the range 13.7–14.7 kbar, as shown in Fig. 1(b). However, beyond ~15 kbar the conductance reduces, regardless of the increasing charge accumulation in the X_Z quantum wells, and this is possibly due to the dominant effect of the depletion barrier which suppresses current flow between the GaAs and AlAs emitter layers when a small bias is applied.

Figure 3 shows the 4.2 K magnetic field dependence of the second derivative of current with respect to bias, measured at 13.7 kbar, just below the type II transition. The zero magnetic field resonance occurring at ~ -0.025 V has been assigned above to the $\Gamma \rightarrow X_Z(1)$ process. The d^2I/dV^2 vs V data are asymmetric about $V=0$. This is probably due to small asymmetries in the sample, such as slightly unequal AlAs thicknesses, and different degrees of interface roughness.[16] At 15 T, up to five additional resonances appear. These magnetic-field-induced resonances are attributed to inter LL processes involving the lowest Γ-symmetry LL in the emitter accumulation layer, with LL index $n_\Gamma=0$, and up to five X-symmetry LL's in the collector AlAs layer, with index $n_X \leqslant 5$. In Fig. 3, the numbers in the parentheses above the peaks indicate the LL indices (n_Γ, n_X). The (0,0) peak is allowed since it involves no change of momentum in the plane, and thus it has a much larger amplitude than the subsequent $(0,n_X)$ peaks, with $n_X \geqslant 1$, which are disorder activated and phonon activated.

At such low bias where the $\Gamma \rightarrow X_Z(1)$ resonance occurs, the 2D electron density in the GaAs Γ triangular potential well is estimated to be less than $1\times10^{11}\,\mathrm{cm}^{-2}$ at all pressures up to the type II transition, using a self-consistent Schrödinger-Poisson calculation.[17] At $B=8$ T, where inter

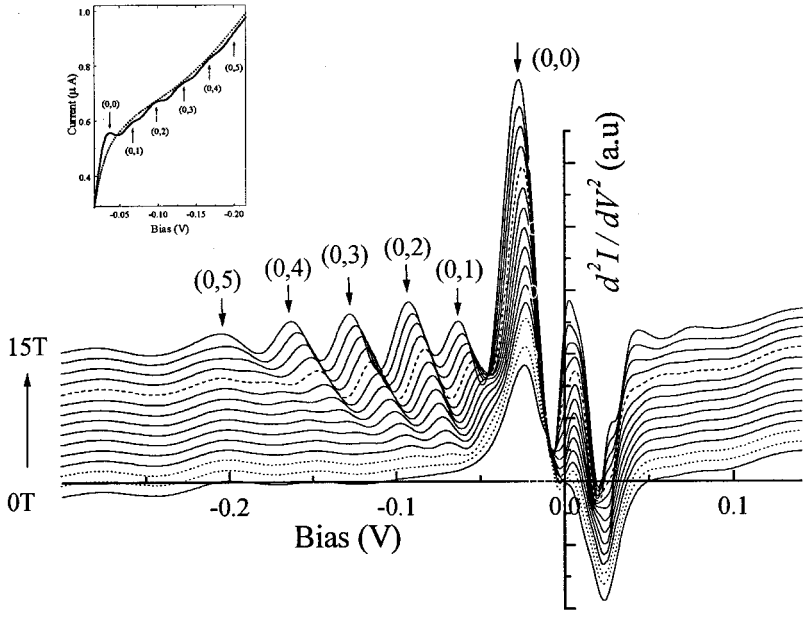

FIG. 3. d^2I/dV^2 vs V characteristics at 13.7 kbar for various magnetic fields, showing the $\Gamma \rightarrow X_Z$ inter Landau level transitions (arrows). The dotted lines show data taken at 7 and 9 T, respectively, and the dashed line represents data at 13 T. Between 9 and 15 T, the field was increased with a step of 0.5 T. The numbers in the parentheses (n_Γ, n_X) indicate the Landau level indices of the emitter and collector states. Inset: current vs voltage (I-V) characteristics at 0 T (dotted) and 15 T (solid). The latter shows clear $\Gamma \rightarrow X_Z$ Landau level features.

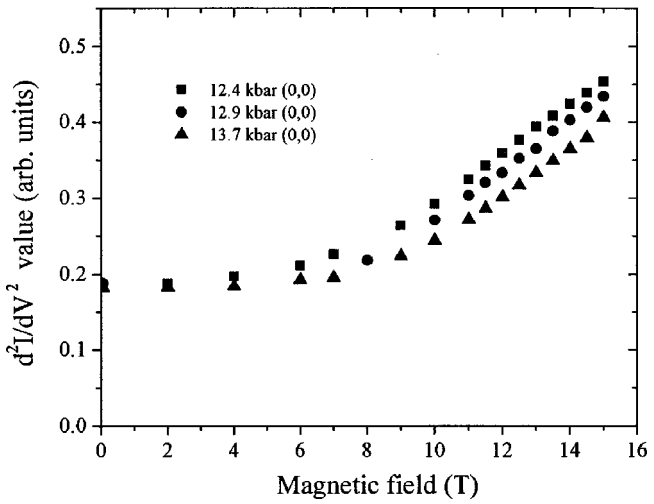

FIG. 4. Magnetic-field dependence of the amplitude of the d^2I/dV^2 peak for the (0,0) Landau level transition, at 12.4 (squares), 12.9 (circles), and 13.7 kbar (triangles). (The points at 2, 4, and 6 T were obtained by numerical differentiation of the conductance data.)

LL tunneling starts to occur, the density of states per Landau level including spin degeneracy is $4\times10^{11}\,\mathrm{cm}^{-2}$, and the Landau level separation ($m^*\sim0.067m_0$) is approximately 13.8 meV. Thus, for the entire set of Landau level transitions measured at 4.2 K, only the $n_\Gamma=0$ emitter Landau level is populated.

Figure 4 shows the field dependence of the amplitude of the d^2I/dV^2 maxima for the (0,0) LL process, measured in the range 12.4–13.7 kbar. The pressure-induced decrease in amplitude at high fixed field is consistent with the reduction in the number of electrons in the Γ emitter accumulation layer at higher pressures. Considering now the amplitude at 13.7 kbar, it is approximately constant until about 8 T, when it starts to increase linearly with field. This linear variation extrapolates back approximately to the origin. Such behavior is to be expected, since in the high-field regime, the strength of the allowed tunneling process should be proportional to the number of states in the lowest collector LL, since the number of electrons in the emitter remains nearly constant. The width of each collector LL, Δ_X can be estimated, since they are just resolved at 8 T. At this field we must have $\Delta_X\approx\hbar\omega_C\approx4$ meV, assuming $m^*_{XY}\approx0.25m_0$.[4]

In Fig. 5(a), two magnified views of the 13.7 kbar d^2I/dV^2 vs V characteristics of Fig. 3 are plotted at 7 T (solid) and 15 T (dotted). At 7 T, elastic and phonon-assisted resonances ($P0$-$P3$) are clearly seen but peaks due to tunneling between LL's do not yet occur. At 15 T, five additional LL peaks are clearly resolved beside the main (0,0) $\Gamma\rightarrow X_Z(1)$ resonance, which are now much stronger than the phonon features observed below 7 T. The bias positions of the maxima of the d^2I/dV^2 vs V characteristics are plotted against magnetic field as circles in Fig. 5(b), revealing a fan of resonances. On the same diagram, the 7 T bias positions of the no-phonon and phonon-assisted resonances are plotted. In the remaining part of the paper we shall make a careful comparison between the bias positions of the phonon peaks and the LL peaks, an approach similar to that used previously for the magnetophonon effect in bulk

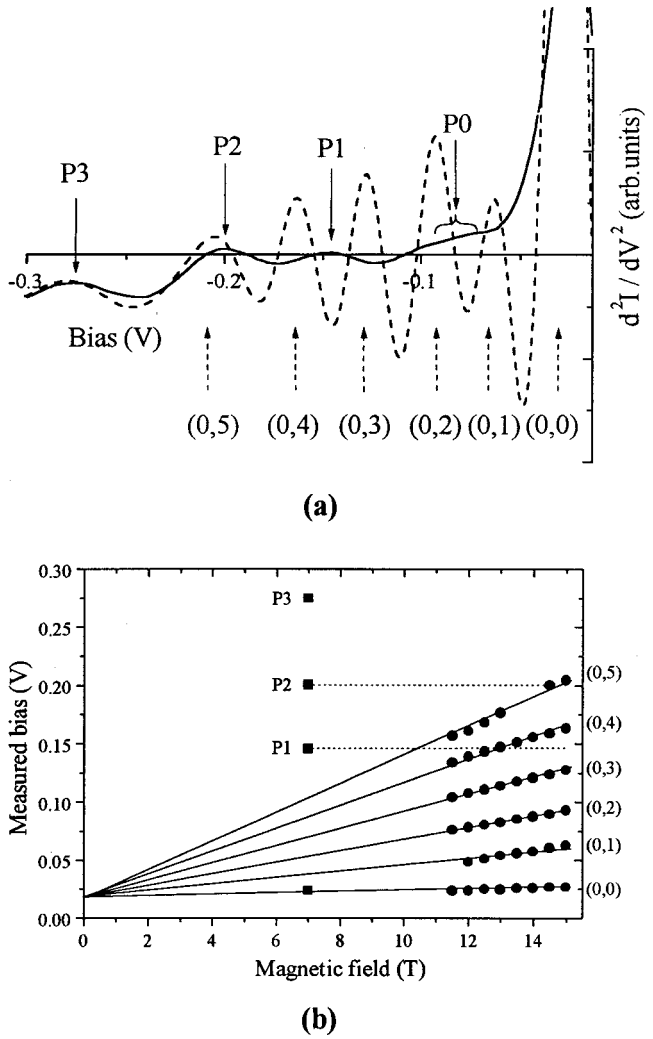

FIG. 5. (a) Magnified view of the reverse bias d^2I/dV^2 vs V measurements of Fig. 3 at 7 T (solid) and 15 T (dotted). At 7 T, the inter-LL transitions are not resolved. (b) Fan diagram for $\Gamma\rightarrow X_Z$ Landau level tunneling at a pressure of 13.7 kbar. The dots show the bias positions of the peaks in the second derivative measurements plotted as a function of magnetic field. Squares indicate the bias positions of the $\Gamma\rightarrow X_Z(1)$ process and its phonon satellites at 7 T. The solid lines are guides for the eye.

semiconductors.[18] This will enable us to obtain an accurate calibration of the cyclotron energy which determines the LL peak separations. From the cyclotron energy we shall make a precise determination of the transverse mass m_{XY}.

First, we relate the applied bias V to the potential difference u between the emitter and collector states

$$V=au^2+bu. \tag{1}$$

This quadratic dependence for $V(u)$ has been proposed previously in Ref. 19. Figure 6 shows that even if the emitter and collector states are nominally aligned at zero applied bias, as expected for pressures above the type II transition, there will still be a small offset potential u_0 due to the broadening of the LL's noted above, since electrons in the emitter will reside in the tail of the partially filled, $n_\Gamma=0$, LL, whereas the first peak in the current will occur when these

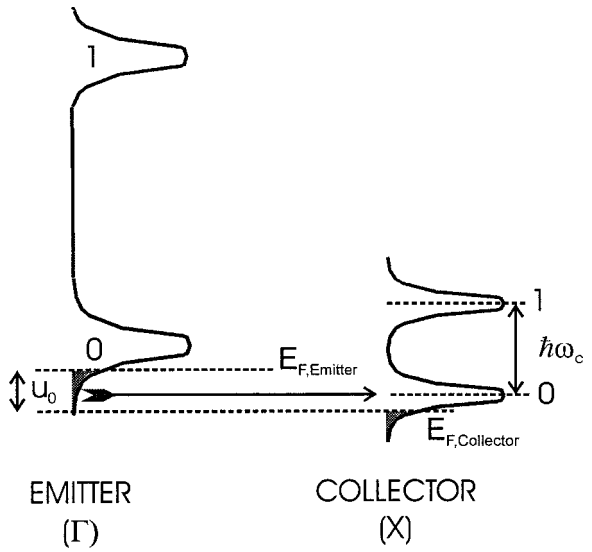

FIG. 6. Schematic diagram showing the alignment of the first two emitter and collector Landau levels when biased to a peak in the resonant current. Even when the lowest Landau levels are nominally aligned at zero bias, a small voltage offset u_0 is required to achieve resonance, due to the finite width of the Landau levels and the low electron population of the emitter.

electrons align with the center of the $n_X=0$ collector LL. For pressures below the type II transition, we shall take u_0 to represent the potential relative to the collector AlAs layer that must be added to the emitter state to align it with the lowest collector state at the first resonance. The offset potential u_0 therefore decreases with increasing pressure up to the type II transition, where it saturates at a minimum value. Therefore we write

$$u=u_0+n_X h\omega_C, \tag{2}$$

where ω_C is the cyclotron frequency of the X_Z electrons. Substitution into Eq. (1) gives

$$V(n_X)=An_X^2+Bn_X+C=A\left[\frac{u-u_0}{h\omega_C}\right]^2+B\left[\frac{u-u_0}{h\omega_C}\right]+C, \tag{3}$$

where the coefficients A, B, and C are easily derived functions of a, b, ω_C, and u_0. Thus we expect that C will reduce with pressure up to the type II transition, but it will not vanish at or above the transition pressure when u_0 has its minimum value, shown in Fig. 6. This behavior is consistent with experiment.

We have fitted the bias values for the LL peaks $(0,n_X)$ with $n_X \geqslant 1$ at five pressures between 11.7 and 14.7 kbar to the first line of Eq. (3), in order to determine the values of A, B, and C at each pressure. In each case, the fit is very good, with an rms deviation between the measured LL bias positions and those predicted by Eq. (3) of between 0.5 and 1 mV, depending on the pressure.

Figure 5 shows the four phonon features observed at 7 T. If the phonon energy is $h\Omega_P$, and the potential difference between emitter and collector states is u, then

$$h\Omega_P=u-u_0, \tag{4}$$

where u_0 is the potential offset due to broadening, as in the case of the Landau levels. In principle, u_0 is a weak function of magnetic field. However, if we assume that $u_0(15\,\mathrm{T})-u_0(7\,\mathrm{T})\approx 0$, then substitution of Eq. (4) into Eq. (3) gives

$$V(n_X)=A\left[\frac{\Omega_P}{\omega_C}\right]^2+B\left[\frac{\Omega_P}{\omega_C}\right]+C. \tag{5}$$

Since A, B, and C are already determined, we may use Eq. (5) to find the cyclotron frequency, if we can identify one of the phonons in Fig. 5 and establish its frequency accurately. By taking the phonon $P2$ to be the GaAs LO(Γ) phonon, we show below that all the other phonon features in Fig. 5 may be correctly attributed, with no room for ambiguity. It turns out that this phonon energy has been determined very precisely, with an error of ± 0.3 meV,[20] and its variation with pressure is also known accurately.[21,22] We can determine the bias position of the $P2$ peak in Fig. 5(a), with an accuracy of ± 0.5 mV, which is comparable to the bias error introduced in fitting the A, B, and C coefficients. Thus, the cyclotron energy $\hbar\omega_C$ and hence the transverse mass value m_{XY} are determined to an accuracy of 2%. Using our value for the cyclotron energy in Eq. (5), we find the other phonon energies with an accuracy of about 3.5%. Note that the error in these phonon energies is greater than that of $P2$, due to the way the errors in $\hbar\omega_C$ and the bias combine. Very consistent results are obtained over the range 11.7–14.7 kbar, which are tabulated in Table I. These phonon energies compare very well with the known values listed along with their known pressure variations in Table II.

The $P0$ feature is very broad, appearing in Fig. 5 as two peaks. The fitted value of this feature at all pressures covers the range $u=(12.5\pm 2.5)$ meV, consistent with the splitting noted in Table II for the GaAs and AlAs TA(X) phonons. The $P4$ feature in Fig. 1(a) gives $u\sim 70$ meV at 14.7 kbar, and is attributed to TA(X) phonon-assisted tunneling between Γ and $X_{XY}(1)$.[9,17] If the final state were $X_Z(1)$, it would lie above any single phonon energy. When comparing Tables I and II, we note that the GaAs LO(X) mode ($h\Omega_P \sim 30.3$ meV at 1 bar) does not appear to participate in the

TABLE I. Summary of the fitted $P1$ and $P3$ phonon energies, and the cyclotron mass $m_{X,Y}$ obtained by using LL's measured at 15 T and phonon peaks measured at 7 T, in the pressure range 11.7–14.7 kbar. The $P2$ phonon energy in the table was used as input data. The energy unit is meV.

	11.7 kbar	12.4 kbar	12.9 kbar	13.7 kbar	14.7 kbar
$P1$	27.2 ± 0.4	27.5 ± 0.4	27.5 ± 0.4	26.7 ± 0.4	26.7 ± 0.4
$P2$	37.1 ± 0.3	37.2 ± 0.3	37.2 ± 0.3	37.3 ± 0.3	37.3 ± 0.3
$P3$		49.1 ± 0.9		50.1 ± 0.9	51.5 ± 0.9
m_{XY}/m_0	0.237 ± 0.002	0.234 ± 0.002	0.231 ± 0.002	0.229 ± 0.002	0.225 ± 0.002

TABLE II. Phonons assigned to the peaks $P0-P3$, with their energies and pressure coefficients from the literature.

Phonon	Assignment	Energy at 1 bar (meV)	Reference	Pressure coefficient (%/kbar) (from Refs. 21 and 22)
$P0$	$TA_{GaAs}(X)/TA_{AlAs}(X)$	10.1/12.7	24	$-0.16/-0.17$
$P1$	$LA_{GaAs}(X)/LA_{AlAs}(X)$	27.9 ± 0.4	20	0.16/0.21
$P2$	$LO_{GaAs}(\Gamma)$	36.6 ± 0.3	20	0.13
$P3$	$LO_{AlAs}(\Gamma)/LO_{AlAs}(X)$	49.7/48.0	20	0.12/0.26

tunneling. This is consistent with its weak scattering between Γ and X states in type II resonant Raman spectra,[20] where its contribution is approximately one order of magnitude smaller than that due to the GaAs LA(X) mode. The reason for this is that the LO(X) mode is confined in the GaAs layers and has a poor overlap with the AlAs collector $X_Z(1)$ state, whereas the LA(X) phonon is not confined by the heterostructure and has a much better overlap both with the $X_Z(1)$ state and the emitter Γ state. Note that the LA(X) phonon has X_3 symmetry and couples to the X_3 component of the $X_Z(1)$ wave function.[15]

The appearance of both zone center (Γ) and zone boundary (X) phonons in the inelastic tunneling indicates either that both GaAs Γ and AlAs $X_Z(1)$ states act as emitter states above 10.8 kbar (see Fig. 1), or that only GaAs Γ acts as the emitter state but that there is a significant admixture between Γ and X_Z states due to Γ-X_Z mixing. The former requires alignment of both GaAs Γ and AlAs $X_Z(1)$ states in the emitter and pinning of their quasi-Fermi levels. This is not possible at 10.8 kbar, since the type II transition occurs near 14 kbar. Therefore Γ-X_Z mixing seems the most likely explanation. This will cause admixture of Γ states in the 40 Å GaAs well, especially the first confined state $\Gamma(1)$ with the collector $X_Z(1)$ state, and also admixture of the $X_Z(1)$ state in the emitter AlAs layer with the Γ emitter state. Such an admixture can explain why the $LO_{GaAs}(\Gamma)$ [and $LO_{AlAs}(\Gamma)$] satellite is observed with similar strength to the features due to X-point phonons. Although the admixture introduces only a small amplitude of the $\Gamma(1)$ state into the collector $X_Z(1)$ state, the Γ emitter state will have a much stronger overlap with this $\Gamma(1)$ state than it does with the confined $X_Z(1)$ state in the AlAs collector layer. Furthermore, the LO(Γ) phonon will couple much more strongly than do the X-point phonons because Fröhlich scattering by small wave-vector (confined) phonons is much stronger than deformation potential scattering by zone boundary phonons. This deformation potential scattering between the emitter Γ and collector $X_Z(1)$ states is responsible for the other phonon satellites which all have zone boundary character.

The very good agreement between the fitted phonon energies in Table I and the energies of the phonons listed in Table II, provides the final confirmation of the initial assignment of $P2$ as the GaAs LO(Γ) phonon and hence confirms the value deduced for the mass, m_{XY}. If a higher mass value is used to calculate the cyclotron frequency in Eq. (5) it reduces the phonon energies and makes it impossible to assign $P1$, since no suitable Γ or X-point phonons exist with 1 bar energies between $\sim$28 and $\sim$12 meV. On the other hand, a lower mass value increases the phonon energies making it impossible to assign $P3$, since no phonons exist at all with 1 bar energies above 50 meV.

Figure 7 shows the variation of the transverse mass m_{XY} with pressure between 11.7 and 14.7 kbar. As pressure is increased, the mass decreases. From a least-squares fit to the points, we find the pressure dependence of the m_{XY} to be $m_{XY}/m_0=(0.282\pm0.004)-(0.0039\pm0.0003)\times P$ where P is the pressure in kbar. The error in the 1 bar value can be understood as follows. In Fig. 7, it is clear that the deviation of the five data points from the fitted line is considerably less than the error bars listed in the last line of Table I, which are mostly due to the ±0.3 meV error in the GaAs LO(Γ) phonon energy. This deviation between the fitted line and the data is essentially due to a combination of the $P2$ bias error and the bias error introduced by fitting the A, B, and C coefficients, and agrees well with that expected from our bias uncertainty in each case of $\sim\pm0.5$ mV. It is this random deviation, therefore, that contributes to the error in the fitted pressure coefficient and 1 bar mass value. The uncertainty in the GaAs LO(Γ) phonon energy will then shift all of the points up or down *together* by about $\pm0.002m_0$. Therefore this uncertainty will provide an additional *systematic* error in the 1 bar value of the mass, which should be added to the random error produced by the least-squares fitting. The mass m_{XY} is thus $(0.282\pm0.006)-(0.0039\pm0.0003)\times P$.

There remains the final point of how valid is our assump-

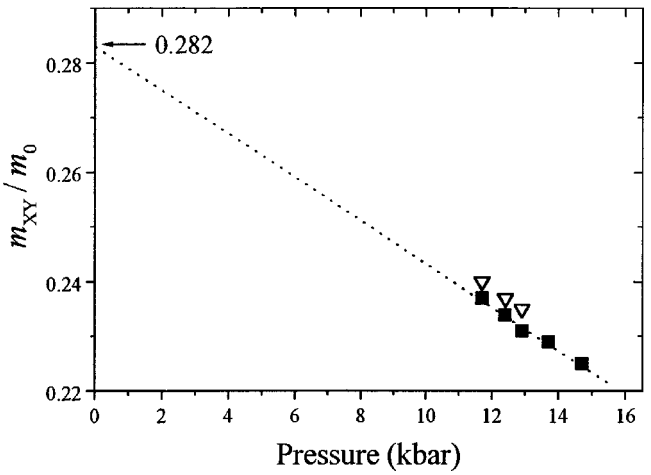

FIG. 7. Pressure dependence of the transverse X-point mass $m_{X,Y}$. The squares are deduced from the 15 T LL peaks and the 7 T peak for the $P2$ phonon. The open triangles are based on LL peaks and the $P2$ phonon peak, all measured at 13 T. The dotted line shows a least-squares fit to the squares.

tion that changes to the broadening parameter u_0 between 7 and 15 T may be ignored. To test this, we note that for the dashed line in Fig. 3, corresponding to 13 T, the $P2$ phonon feature may just be identified separately from the (0,5) LL, whereas it cannot be resolved at higher fields. Therefore, we have performed the same analysis as above using only the results measured at 13 T to determine the bias positions of both the $P2$ phonon and the LL peaks. We have not included points above 13 kbar in the 13 T analysis, because the increase in the cyclotron energy with pressure causes the (0,5) LL to come too close to the $P2$ peak above this pressure to allow an accurate determination of either bias position. The results below 13 kbar, however, are plotted as open triangles in Fig. 7, and are found to lie $\sim 0.003m_0$ above the results determined using the phonon peak at 7 T. This error is well within that of $\pm 0.006m_0$ just determined above and may simply be due to the greater inaccuracy in determining both the $P2$ and LL peaks from the same 13 T data where they are not as well resolved as they are separately at 7 and 15 T, respectively. However, since it could also be argued that the error may be due to a variation of u_0 with magnetic field, it places an extra *systematic* uncertainty on our result of up to $+0.003m_0$ due to a possible breakdown in the assumption $u_0(15\,\mathrm{T}) - u_0(7\,\mathrm{T}) \approx 0$. Therefore to take this into account we must increase the mass value by $0.0015m_0$ and add a further uncertainty to the final result of $\pm 0.0015m_0$. The final determination of the mass m_{XY} is thus

$$\frac{m_{XY}}{m_0} = (0.284 \pm 0.008) - (0.0039 \pm 0.0003) \times P. \qquad (6)$$

Our determination should be compared with two recent determinations which appear to span a fairly wide range. Finley *et al.*[9] obtained $(0.28 \pm 0.03)m_0$ using the same $\Gamma \rightarrow X_Z(1)$ tunneling at 1 bar through a single AlAs barrier in a large electric field. On the other hand Smith *et al.* reported $(0.25 \pm 0.03)m_0$, by fitting the bias value of the $X_{XY}(1) \rightarrow X_{XY}(2)$ tunneling process at an average pressure of ~ 7 kbar, using a self-consistent Schrödinger-Poisson model.[4] Both determinations agree very well with Eq. (6), however, if the pressure at which each was made is taken into account.

Our new determination for the mass m_{XY} is much more accurate than any previous determination, due to our method of calibration using an accurately determined phonon energy. We have also determined the pressure dependence. We note that it is surprisingly large, at -1.4%/kbar, more than twice the variation of the Γ-point electron mass and with the opposite sign.[23]

IV. SUMMARY

We have investigated resonant tunneling between Γ and X_Z states in a GaAs/AlAs double barrier structure, using hydrostatic pressure and a magnetic field applied perpendicular to the interfaces. The well and barrier of dimensions are such that at pressures below the type II transition, resonant tunneling may be observed between a Γ state in the emitter accumulation layer and the confined $X_Z(1)$ state in the collector AlAs layer. Above the transition pressure, tunneling from the confined $X_Z(1)$ state in the emitter AlAs layer may also be seen. By comparing the bias positions of tunneling features due to phonons and those due to inter Landau level tunneling, we have made an unambiguous assignment of the phonons involved. Both zone center and zone boundary phonons have been observed, highlighting the involvement of Γ-X_Z mixing of electron states in the former case. From an accurate knowledge of the GaAs LO(Γ) phonon energy, we have calibrated the cyclotron energy in a manner analogous to that used to interpret the magnetophonon effect in bulk semiconductors. We have thereby determined the value of the transverse X-point effective mass in AlAs to a much greater accuracy than previously: $m_{XY} = (0.284 \pm 0.008)m_0$. We have also determined its pressure dependence, finding a strong decrease with pressure: $dm_{XY}/dP = -(0.0039 \pm 0.0003)m_0$/kbar. This strong negative pressure dependence explains the fairly wide range of the values reported recently, which were based on measurements made at different pressures.

ACKNOWLEDGMENTS

This work was funded by the Engineering and Physical Sciences Research Council (EPSRC) of the U.K. We also thank Professor M. E. Eremets for assistance with preparing the pressure cell.

*Fax: 44-1865-272400, Email address: p.klipstein@physics.ox.ac.uk.

[1] E. E. Mendez, L. Esaki, and W. I. Wang, Phys. Rev. B **33**, 2893 (1986).

[2] J. Smoliner, E. Gornik, and G. Weimann, Phys. Rev. B **39**, 12 937 (1989).

[3] D. G. Austing, P. C. Klipstein, J. S. Roberts, C. P. Mistry, and G. Hill, J. Appl. Phys. **74**, 7340 (1993).

[4] J. M. Smith, P. C. Klipstein, R. Grey, and G. Hill, Phys. Rev. B **57**, 1740 (1998).

[5] H. Im, P. C. Klipstein, J. M. Smith, R. Grey, and G. Hill, Phys. Status Solidi B **211**, 489 (1999).

[6] J. M. Smith, P. C. Klipstein, R. Grey, and G. Hill, Phys. Rev. B **57**, 1746 (1998).

[7] H. W. van Kesteren, E. C. Cosman, P. Dawson, K. J. Moore, and C. T. Foxon, Phys. Rev. B **39**, 13 426 (1989).

[8] H. Im, P. C. Klipstein, R. Grey, and G. Hill, in *Proceedings of the 24th International Conference on the Physics of Semiconductors*, edited by M. Heiblum and E. Cohen (World Scientific, Singapore, 1998), CD-ROM file: 1075.pdf (1999).

[9] J. J. Finley, R. J. Teissier, M. S. Skolnick, J. W. Cockburn, R. Grey, G. Hill, and M. A. Pate, Phys. Rev. B **54**, R5251 (1996).

[10] H. Im, P. C. Klipstein, R. Grey, and G. Hill, Phys. Rev. Lett. **83**, 3693 (1999).

[11] H. Im, L. E. Bremme, P. C. Klipstein, A. V. Kornilov, R. Grey, and G. Hill, in Proceedings of the 25th International Conference on the Physics of Semiconductors, Osaka, 2000 (Springer-Verlag, in press).

[12] O. Madelung, *Semiconductors: Basic Data* (Springer, New York, 1996), p. 76.

[13] L. E. Bremme, H. Im, H. Choi, P. C. Klipstein, G. W. Smith, and R. Grey, Proceedings of the 25th International Conference on

the Physics of Semiconductors (Ref. 11).
[14] M. E. Eremets (private communication).
[15] P. C. Klipstein, in *High Pressure Semiconductor Physics II*, edited by T. Suski and W. Paul, Semiconductors and Semimetals Vol. 55 (Academic, New York, 1998), Chap. 2, p. 45.
[16] Based on the discussion in Ref. 15, the $\Gamma \rightarrow X_Z(1)$ resonance can be described in terms of quantum beats, in which the beat frequency depends essentially on the Γ-X_Z mixing caused by the interface of the collector AlAs layer that is closest to the emitter. This mixing is very sensitive to the degree of interface roughness.
[17] Hyunsik Im, Ph.D. thesis, Clarendon Laboratory, Oxford University, 1999.
[18] R. A. Stradling and R. A. Wood, J. Phys. C **1**, 1711 (1968).
[19] D. G. Austing, P. C. Klipstein, A. W. Higgs, H. J. Hutchinson, G. W. Smith, J. S. Roberts, and G. Hill, Phys. Rev. B **47**, 1419 (1993).
[20] W. R. Tribe, P. C. Klipstein, G. W. Smith, and R. Grey, Phys. Rev. B **54**, 8721 (1996).
[21] D. N. Talwar and M. Vandervyver, Phys. Rev. B **41**, 12 129 (1990).
[22] H.-M. Kagawa and T. Soma, Solid State Commun. **62**, 707 (1987).
[23] Z. Wasilewski and R. A. Stradling, Semicond. Sci. Technol. **1**, 264 (1986).
[24] S. Adachi, *GaAs and Related Materials: Bulk, Semiconducting and Superlattice Properties* (World Scientific, Singapore, 1994).